Journal Name

Dynamic Article Links ►

Cite this: DOI: 10.1039/c0xx00000x

www.rsc.org/xxxxxx

Paper

Fabrication, structure and mechanism of reduced graphene oxide based carbon composite films

Yongan Niu,[a] Xin Zhang,[b] Jiupeng Zhao,[b] Yanqing Tian,[c] Xiangqiao Yan,[a] and Yao Li*[a]

Received (in XXX, XXX) Xth XXXXXXXXX 20XX, Accepted Xth XXXXXXXXX 20XX

DOI: 10.1039/b000000x

This work suggested an effective approach to fabricating the reduced graphene oxide based carbon (RGO/C) composite films. Carbonization of graphene oxide reinforced polyimide (GO/PI) composite films were investigated by the thermogravimetric analysis (TGA) and differential scanning calorimetry (DSC). Crystalline structures and carbonized mechanism of the RGO/C composite films were investigated in detail by an X-ray diffraction (XRD) and Fourier transform infrared spectroscopy (FTIR). Furthermore, the carbonization yields were improved due to catalytic effects of RGO. These RGO/C composite films exhibited the obvious structural orientations by SEM investigation of their cross sections.

1. Introduction

Graphene and graphene oxide (GO) based composites were considered as the most promising materials due to their extensive and potential applications, i. e. electric devices [1], catalysis[2], solar cells [3] and even aerospace elevator [4]. Recently, many researchers have made several rapid progresses toward preparing the GO or RGO based composites and developing their outstanding properties, including epoxy (EP) [5], phenol formaldehyde (PF) [6], polyimide (PI) [7], polyvinylidene fluoride (PVDF) [8], polyaniline (PANI) [9] and silicon (SI) resins [10].

As we known, the PI films [11~13] were considered to be suitable as the high-effective precursors of carbonized films, owing to their thermal conductivity, tensile modulus and strength, optical and electrical properties [14]. Therefore, as significant electrical materials [15] and electrodes [16], the RGO/C composites prepared by carbonization of GO/PI composites could provide the higher critical electron-delivery efficiency and structural strengths than traditional carbon materials. However, to fabricate the high-performance RGO/C composite films, a serious challenge was the terrible compatibility between GO sheets and PI film [17]. The influence of RGO sheets on carbonization of GO/PI composite films was also another challenge in this area.

In this work, we developed a facile ultra-sonicate method [18] to prepare the steady GO suspensions. The GO/PI composites films with different GO contents were obtained by an in situ polycondensation from 3,3',4,4'-benzophenonetetracarboxylic dianhydride (BTDA) and 4,4'-diamino-diphenyl ether (ODA). Subsequently, RGO/C composite films were fabricated by carbonization of GO/PI composite films at 400, 600, 800 and 1000^{o}C, respectively. The carbonization yields are calculated by the mass changes. The structures and fracture toughness of these films also are investigated by XRD patterns, FTIR spectra and SEM micrographs.

2. Experimental

2.1 Materials

All agents were analytical reagent (AR) grade and used as received without further purification. Natural graphite was purchased from Qingdao graphite materials Co. Ltd. N, N-dimethylacetamide (DMAC) and ethylenediamine (EDA) were purchased from Tianjin Chemical Reagent Co. Ltd. BTDA and ODA (>99.9%) were obtained from China Sinopharm Chemical Reagent.

2.2 Preparation of GO/PI composites films

Graphite oxide was synthesized by modified Hummers method from natural graphite [19]. The steady GO suspension in DMAC at a concentration of 2 mg/mL was prepared under the sonication for 60 min and modified by EDA. The calculated DMAC solvents and GO suspensions, i. e. GO ratios of 0.25wt%, 0.5wt%, 1.0wt% and 2.0wt%, were added to a clean three-neck flask. Subsequently, 0.01mol of ODA was putted into the flask and dissolved in the mixture solvent. After stirring for 30min, 0.0102mol of BTDA was added into this flask in batches. Uniformly stirring for 5h, GO and polyamic acid (GO/PAA) solutions were synthesized. The GO/PI composite films were prepared under the curing conditions of 60^{o}C for 3h, 100^{o}C for 1h, 200^{o}C for 1h and 300^{o}C for 2h in a curing oven.

2.3 Preparation of RGO/C composite films

Before the carbonization of GO/PI composite films, post-treatment at the temperature of 400^{o}C for 1h was made to remove small molecules in these films. The above GO/PI composite films were firstly cut into square of 20mm×20mm and stacked together and putted into the middle of two quartz plates. Carbonization of the GO/PI composite films was took place in the constant temperature area of a vacuum tube furnace (OFX-1500X) at a heating rate at 2^{o}C/min, under a nitrogen (N_2) flowing rate of 10L/min and at 400, 600, 800 and 1000^{o}C for 2h, respectively.

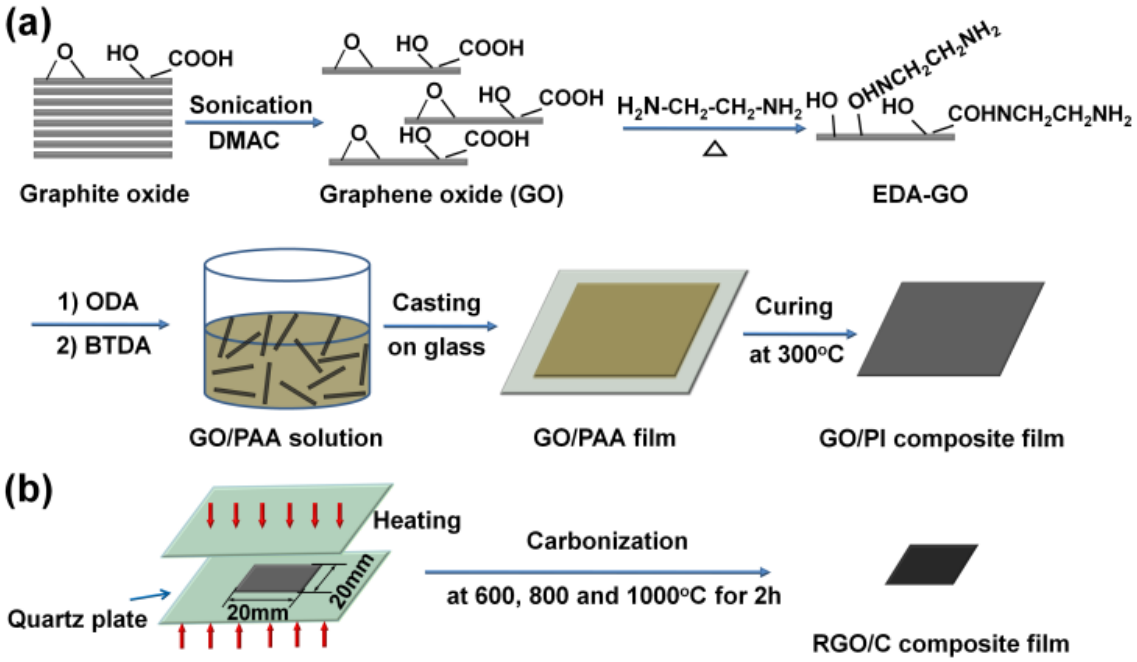

Fig. 1 Schematic illustrations of preparation of (a) GO/PI composite films and (b) RGO/C composite films.

The RGO/C composite films were obtained after these two processes and their mass changes were recorded in the same time. Fig. 1 showed schematic illustration of the prepared process and carbonized process of GO/PI composite films.

2.4 Characterizations

Carbonization processes of polyimide and GO/PI composites films were analyzed according to the changes of mass loss and thermal flow by a TGA analysis and DSC (STA 449C, Netzsch Co.) experiment, under the N_2 atmosphere at a heating rate of 10oC/min from room temperature to 1500°C [20]. Crystalline grains and structures of these films were investigated by a XRD technique (Dmax-rB 12kW, Rigaku Co., Ltd.) with Cu Kα radiation (λ = 1.5406Å) and Raman spectroscopy (HR 800, Olympus Co.). The chemical compositions and molecular structure of the GO/PI and RGO/C composites films were characterized by a Fourier transform infrared spectroscopy (FT-IR, Avatar-360, Nicolet Co.). The cross sectional morphologies and fracture toughness of the carbonized films were investigated by a SEM technique (Quanta 200FEG, FEI Co.).

3 Results and Discussion

To analyze the carbonization process, Fig. 2 displayed the TGA curves of GO/PI films in N_2 atmosphere. The pyrolysis of GO sheets was divided into two steps, as our previous report [21]. The first step was under the temperature of 200°C, assigned to the decomposition of oxygen functional groups, i.e. -C=O, -OH and epoxy group. The GO sheets could transform to the RGO sheets. The second step was ranged from 500°C to 750°C, which is related to the structural reorganization and densification.

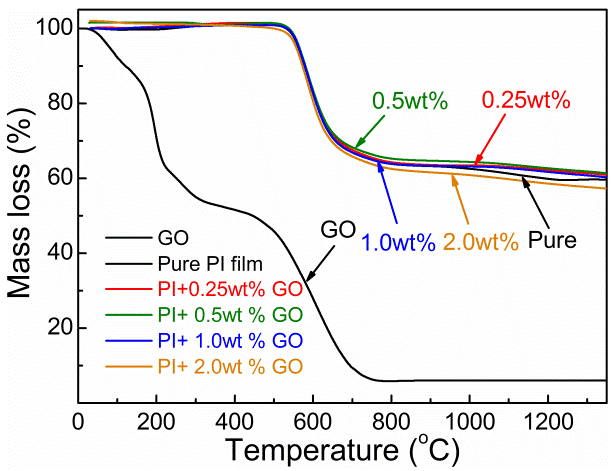

Fig. 2 TGA curves of the GO, pure PI and GO/PI composite films with different GO contents.

Pure PI film contained a large amount of benzene and imide groups in their main chains, which provided its higher pyrolysis temperature, exceed 550°C. The thermal stabilities of GO/PI composite films were enhanced with the increase of GO loadings below 0.5wt%, because the good interfaces between GO (or RGO) sheets and PI molecules improved their compatibility and leaded to the increase of cohesive energy [22]. However, with the GO contents exceeding 1.0wt%, the pyrolysis rate of GO/PI composite films would be accelerated. Because the GO sheets have lower thermal stability than PI matrix. Herein, the carbonization yield had a slight reduction, due to the pyrolysis of GO (or RGO) sheets.

Combining with DSC curves in Fig. 3, it obviously demonstrated that these PI and GO/PI composite films were two endothermic peaks: the pyrolysis temperature between 400°C and 600°C, corresponding to the degeneration of micro-molecules in branch

chains, and the carbonized temperature between 800 and 1300°C, corresponding to reorganization and carbonization of the main chains in polyimide molecules [23]. In particular, for GO/PI composite films with 0.5wt% GO contents, the pyrolysis temperature was at 678.8°C (T_{d10}), higher than the others. The prime reason was the GO sheets could bring to more aromatic units and prevent release of as-produced small molecules [24]. For pure PI film, the carbonized temperature was at 1250°C. In this process, for GO/PI composite films with 0.5wt% GO contents, its carbonized temperature was reduced to 884.0°C, lower than the others, owing to the presence of GO (or RGO) sheets. However, exceeding 0.5wt%, GO (or RGO) sheets would hinder the carbonized progress of GO/PI composite films, because of the decreasing of GO sheets dispersed in PI films [25]. Therefore, the GO (or RGO) sheets would accelerate carbonized process of GO/PI composite films and improve the efficiency and atom economy.

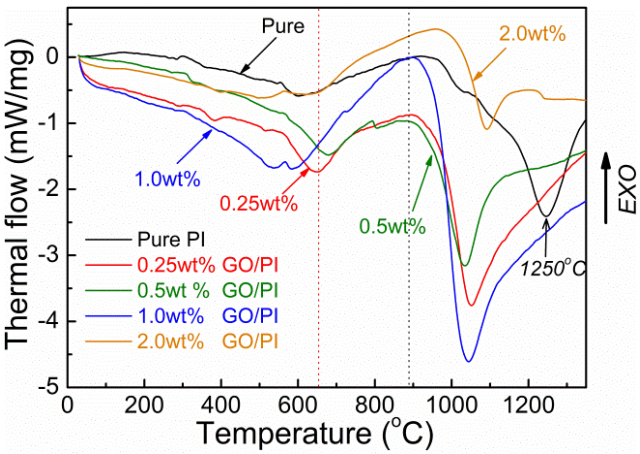

Fig. 3 DSC curves of the pure PI and GO/PI composite films with different GO contents.

To describe the structural evolutions, Fig. 4 showed the FTIR spectra of the GO/PI composite films carbonized at different temperatures. Fig. 4a obviously demonstrated that the structures of PI and GO/PI composite films have no significant changes annealed at 400°C. However, with the increasing of the GO contents, the absorption peak at 1630cm^{-1}, attributed to C=C bonds in aromatic groups, had be divided to two small peaks, highlighted by bi-arrows. This change was associated with the strong interfacial interactions between RGO sheets and aromatic groups in main chains of PI molecules [26]. In this case, it indicated that the reorganization of RGO sheets and PI molecules was happened and intensified with the increasing of GO contents.

As shown in Fig. 4b, the chemical compositions of the carbonized films were quickly changed. For GO/PI composite films of 5wt% GO content, the absorption peak strength at 1720cm^{-1}, assigned to C=O bond, was enhanced, compared with other GO/PI composite films. These characteristics were agreement with the thermal stabilities of GO/PI composite films in TGA and DSC curves. Furthermore, as shown in Fig. 4c and Fig. 4d, the absorption peak at 1570cm^{-1}, assigned to aromatic groups, became the main presence of these composite films, where carbonized temperatures reached up to 800 and 1000°C. It indicated that the RGO/C composite films were successfully obtained at 1000°C for 2h.

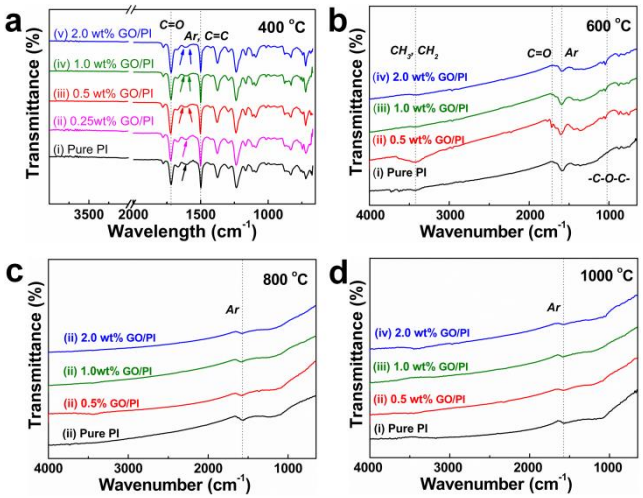

Fig. 4 FTIR spectra of RGO/C composite films carbonized at 400, 600, 800 and 1000°C for 2h.

Fig. 5 showed the related curves of average carbonization yields with the changes of the temperature and GO contents. Although RGO sheets were unstable exceed 800°C, the carbonization yield at 1000°C also reaches up to 58.5% for the GO/PI composite films with a 0.5wt% GO content. In this process, carbonized process was accelerated by catalytic effects of the RGO sheets. However, two main factors could enlarge their carbonization yield. One factor was that RGO sheets play a similar background role on the carbonization, due to their honeycomb-like stacked structures [27]. Moreover, due to accelerating the pyrolysis rate, the small molecules were easily released as a saturated state, such as hydrogen (H_2) and N_2. Here, the outstanding atomic economy was exhibited in carbonized process of GO/PI composite films.

XRD patterns were measured to investigate the crystalline structures of RGO/C composite films, as shown in Fig. 6. All the patterns at 400°C presented an obvious diffraction peak of 2θ located at 19.1°, assigned to the structural orientation of PI molecules [28]. The crystalline spacing (d-spacing) of (002) could be calculated by Bragg's equation:

$$n\lambda = 2d\sin\theta \quad (1)$$

Where d is the crystalline spacing of samples; n=1 is an integer of first order reflection; λ=1.5406nm is the X-ray wavelength of Cu kλ radiation; θ is the Bragg angle.

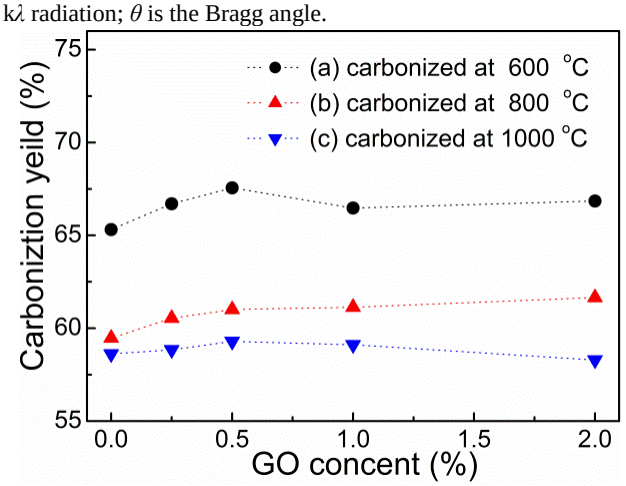

Fig. 5 Carbonization yields of pure PI and GO/PI composite films

carbonized at 600, 800 and 1000°C for 2h.

The intensities of RGO/PI composite films (in Fig. 6a) were gradually enhanced with the increase of GO contents and the corresponding *d*-spacing was increasing from 4.766 Å to 4.736 Å.

During the carbonization at 600°C, the diffraction peak shifted to about 2θ=21°, corresponding to the above amorphous structures carbonized at 400°C. With the increasing of GO content, an obvious 2θ peak at 11.6° appeared, assigned to the (002) feature peak of the thermal reduced GO sheets. Carbonized at 800 and 1000°C, the (002) feature peak of RGO sheets were presented in XRD patterns of RGO/C composite films, as shown in Fig. 6c and Fig. 6d. The (002) peak of the carbonized films of pure PI films became narrower and sharper. It indicated that their structures were near to that of graphite at 2θ=26.1° [29]. Meanwhile, the *d*-spacings calculated from (002) peaks of RGO/C composite films were 3.639, 3.735, and 3.867Å, for GO contents of 0.5wt%, 1wt% and 2wt%, respectively. Therefore, the catalytic effects of RGO sheets could improve the crystalline structure of RGO/C composite films. The fracture toughness also would be promoted due to the presence of RGO sheets.

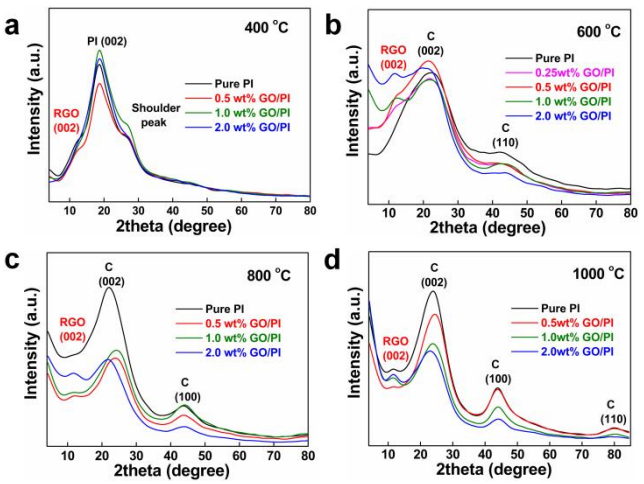

Fig. 6 XRD patterns of RGO/C composite films carbonized at (a) 400, (b) 600, (c) 800 and (d) 1000°C for 2h.

Carbon materials exhibited a high Raman active, which could characterize the different bonding states and the different crystalline forms [30]. Fig. 7 showed the Raman spectra of different carbonized films (RGO/C composite) at 600, 800 and 1000°C for 2h. All the carbonized film presented two intensive scatting peaks, which are assigned to D band at 1360cm^{-1} (assigned to the unordered defects) and G band at 1580 cm^{-1} (assigned to ordered honeycomb structures). And the presences of the second scatting peaks at 2750 and 3100cm^{-1} indicated that these carbonized films were amorphous glassy-carbon structures. Especially, D'' peak at 3100cm^{-1} indicated that the defects were presented in the crystalline edges [31].

The crystalline size (L_a) can be calculated as follows:

$$L_a = 44/(I_D/I_G) \quad (2)$$

Where L_a is calculated crystalline size along a-axis direction, I_D/I_G is the intensity ratio of D band and G band [32].

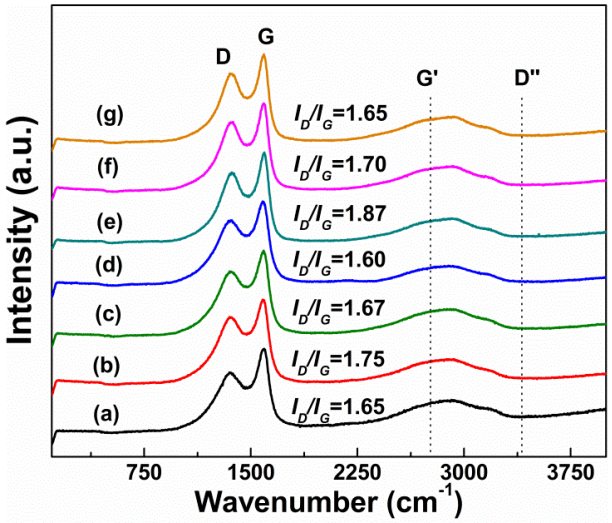

Fig. 7 Raman spectra of RGO/C composite films carbonized at different temperature: (a) pure PI film at 600°C, (b) pure PI film at 800°C, (c) 0.5wt % GO/PI composite film at 800°C, (d) 2wt% GO/PI composite film at 800°C, (e) pure PI film at 1000°C, (f) 0.5wt% GO/PI composite film at 1000°C and (g) 2wt% GO/PI composite film at 1000°C for 2h.

Table 1 showed the calculated results of scattering peak, intensity ratios and crystalline sizes (L_a) according to Raman spectra. Obviously, the crystalline sizes in the direction of L_a were gradually reduced with the increasing of carbonized temperature. However, the crystalline size obviously became larger with the increasing of GO contents. It indicated that RGO sheets might improve the orientation along the direction plane. For 2wt% GO content, the calculated value of L_a reaches would reach to 23.53 nm. The pryolysis of polyimide was took place in a closed inert atmosphere, thus the release of smaller molecules would break out and reduce the "carbonized phase" [33]. However, added the two-dimensional (2-*D*) GO (or RGO) sheets, this broken process would be hindered structure stability would be improved.

The cross-sectional morphologies of the carbon materials were widely evaluated the fracture toughness. Fig. 8 displayed the SEM micrographs of cross sections of the RGO/C composite films carbonized at 1000°C. The fracture mode of pure carbon film was brittle fracture in the Fig. 8a, owing to presence of the smooth fracture surface of glassy carbon. With the increasing of GO contents, the fracture modes of RGO/C composite films had gradually transformed to the dimple rupture processes, as shown in Fig. 8b, 8c, 8d and 8e. The RGO sheets and carbonized district were well combined and homogeneously distributed. Foremost, the obvious transversal cracks were presented in RGO/C composite films of 2.0wt% GO content, as shown in Fig. 8f, which might cause the transgranular cleavage [34]. It was an important evidence of dimple rupture cracks around the RGO sheets, signed by the red arrows. Therefore, it was believed that the RGO sheets obviously enhanced the fracture toughness of the RGO/C composite films.

Table 1 Calculated results of Raman scattering peaks and crystalline sizes for carbonized films at different temperature. (a) pure PI film at 600°C, (b) pure PI film (c) 0.5wt % and (d) 2wt% GO/PI composite film at 800°C, (e) pure PI film, (f) 0.5wt% GO/PI composite film and (g) 2wt% GO/PI composite film at 1000°C for 2h.

Sample	Raman shift/cm^{-1}				I_D/I_G	L_a/nm
	D band	FWHM	G-band	FWHM		
(a)	1355	97	1593	67	1.37	32.12
(b)	1350	89	1582	63	1.75	25.14
(c)	1350	93	1589	67	1.67	26.35
(d)	1358	96	1586	48	1.60	27.50
(e)	1365	87	1588	64	1.87	23.53
(f)	1361	86	1583	59	1.70	25.88
(g)	1363	93	1585	62	1.65	26.67

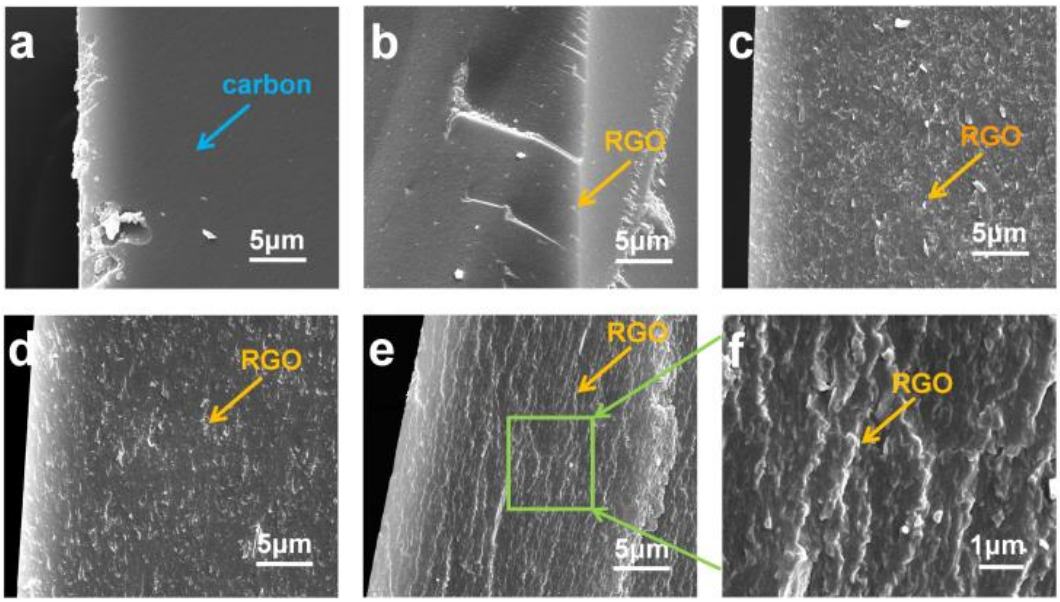

Fig. 8 SEM micrographs of cross sections of (a) carbon films, RGO/C composite films carbonized at 1000°C for 2h with (b) 0.25wt%, (c) 0.5wt%, (d) 1.0wt% and (e) 2.0wt% GO contents, (f) the enlargement of the green district highlighted in (e).

4. Conclusions

In summary, we reported an effective approach to fabricate the RGO/C composite films. The results of thermal analysis demonstrated that the RGO sheets could accelerate the carbonized reaction rate during the carbonization of GO/PI composite films and improve the carbonization yields. Meanwhile, the structural orientations of RGO/C composite films were also improved. The crystalline sizes were grown with the increasing of GO contents. The excellent fracture toughnesses were displayed in these RGO/C composite films. It would be valuable to enlarge the applications of carbon based composite films.

Acknowledgments

We thank National Natural Science Foundation of China (No. 51010005, 91216123, 51174063), the program for New Century Excellent Talents in University (NCET-08-0168). Natural Science Funds for Distinguished Young Scholar of Heilongjiang Province. The project of International Cooperation supported by Ministry of Science and Technology of China (2010DFR50160).

Notes and references

[a] *Harbin Institute of Technology, Center for Composite Materials, Harbin 150001, P. R. China. Fax: 86 451 8640 3767; Tel: 86 451 86402345; E-mail: niuyongan@gmail.com and yaoli@hit.edu.cn*

[b] *Harbin Institute of Technology, School of Chemical Engineering and Technology, Harbin, 150040, P. R. China.*

[c] *Arizona State University, Center for Ecogenomics, Biodesign Institute, Tempe 85287 Arizona, United States*

† Electronic Supplementary Information (ESI) available: [details of any supplementary information available should be included here]. See DOI: 10.1039/b000000x/

‡ Footnotes should appear here. These might include comments relevant to but not central to the matter under discussion, limited experimental and spectral data, and crystallographic data.

1 K. S. Kim and S. J. Park, *Electrochim. Acta*, 2011, **56**, 6547.
2 R. R. Nair, M. Sepioni, I. L. Tsai, O. Lehtinen, J. Keinonen, A. V. Krasheninnikov, T. Thomson, A. K. Geim and I. V. Grigorieva, *Nat. Phys.*, 2012, **8**, 199.
3 Y. W. Zhu, S. Murali, W. W. Cai, X. S. Li, J. W. Suk, J. R. Potts, R. S. Ruoff, *Adv. Mater.*, 2010, **22**, 3906.
4 A. K. Geim and K. S. Novoselov, *Nature Mater.*, 2007, 6, 183.
5 A. P. Yu, P. Ramesh, M. E. Itkis, E. Bekyarova and R. C. Haddon, *J. Phys. Chem. C*, 2007, **111**, 7565.
6 K. Zhang, B. T. Ang, L. L. Zhang, X. S. Zhao and J. H. Wu, *J. Mater. Chem.*, 2011, **21**, 2663.
7 Y. A. Niu, X. Zhang, W. Z. Pan, J. P. Zhao, Y. Li. *RSC Adv.*, 2014, **4**, 7511.
8 J. W. Shang, Y. H. Zhang, L. Yu, X. H. Luan, B. Shen, Z. L. Zhang, F. Z. Lv, P. K. Chu. *J. Mater. Chem. A*, 2013,1, 884-890.
9 Q. F. Lü, Z. W. He, J. Y. Zhang and Q. L. Lin, *J. Anal. Appl. Pyrolysis*, 2012, **93**, 147.
10 R. Verdejo , F. B. Bujans, M. A. R. Perez, J. A. de Saja and M. A. L. Manchado, *J. Mater. Chem.*, 2008, **18**, 2221.
11 V. E. Yudin , M. Y. Goykhman, K. Balik, P. Glogar, G. N. Gubanova and V.V. Kudriavtsev, *Carbon*, 2000, **38**, 5.
12 N. Ohta, Y. Nishi, T. Morishita, T. Tojo and M. Inagaki, *Carbon*, 2008, **46**, 1350-1357.
13 K. Q. Jian, H. Q. Xianyu, J. Eakin, Y. M. Gao, G. P. Crawford and R. H. Hurt, *Carbon*, 2005, **43**, 407.
14 A. C. Lua and J. C. Su, *Carbon*, 2006, **44**, 2964.
15 A. N. Marquez, R. Romero, A. Romeroa and J. L. Valverde, *J. Mater. Chem.*, 2011, **21**, 1664.
16 W. S. Jang, S. S. Chae, S. J. Lee, K. M. Song and H. K. Baik, *Carbon*, 2012, **50**, 943.
17 D. Chen, H. Zhu, T. X. Liu. *ACS Appl. Mater. Interfaces*, 2010, **2**, 3702–3708
18 S. J. Park, J. H. An, I. Jung, R. D. Piner, S. J. An, X. S. Li, A. Velamakanni and R. S. Ruoff, *Nano. Lett.*, 2009, **9**, 1593.
19 S. Stankovich, D. A. Dikin, G. H. B. Dommett, K. M. Kohlhaas, E. J. Zimney, E. A. Stach, R. D. Piner, S. B. T. Nguyen and R. S. Ruoff, *Nature*, 2006, **442**,282.
20 C. Valles, J. D. Nunez, A. M. Benito and W. K. Maser, *Carbon*, 2012, **50**, 835.
21 Y. A. Niu, J. P. Zhao, X. Zhang, X. J. Wang, J. Wu, Y. Li and Y. Li, *Appl. Phys. Lett.*, 2012, **101**, 181903.
22 N. Hu , L. Wei, Y. Wang, R. Gao, J. Chai, Z. Yang, E. S. Kong and Y. Zhang, *J. Nanosci. Nanotechnol.*, 2012, **12**, 173.
23 H. Seyedjamali and A. Pirisedigh, *Polym. Bull.*, 2012, **68**, 299-308.
24 E. R. Margine, M. L. Bocquet and X. Blase, *Nano. Lett.*, 2008, **8**, 3315.
25 J. Y. Wang, S. Y. Yang, Y. L. Huang, H. W. Tien, W. K. Chin and C. C. M. Ma, *J. Mater. Chem.*, 2011, **21**, 13569.
26 W. H. Liao , S. Y. Yang , J. Y. Wang , H. W. Tien , S. T. Hsiao , Y. S. Wang , S. M. Li , C. C. M. Ma, Y. F. Wu, *ACS Appl. Mater. Interfaces*, 2013, **5**, 869–877.
27 K. P. Loh, Q. L. Bao, G. Eda and M. Chhowalla, *Nat. Chem.*, 2010, **2**, 1015.
28 T. Agag, T. Koga and T. Takeichi, *Polymer*, 2001, **42**, 3399-3408.
29 L. Zhao, Y. J. Qiu, J. Yu, X. Y. Deng, C. L. Dai and X. D. Bai, *Nanoscale*, 2013, **5**, 4902.
30 A. Dasari, Z. Z. Yu and Y. M. Mai. *Polymer*, 2009, **50**, 4112.
31 A. C. Ferrari, *Solid State Comm.*, 2007, 143, 47.
32 M. A. Pimenta, A. Jorio, L. G. Cancado, G. Dresselhaus, M. S. Dresselhaus and R. Saito. *Phys. Chem. Chem. Phys.*, 2007, **9**, 1276.
33 C. Berger, Z. M. Song, T. B. Li, X. B. Li, A, Y. Ogbazghi, R, Feng, Z. T. Dai, A. N. Marchenkov, E. H. Conrad, P. N. First and W. A. de Heer. *J. Phys. Chem. B.*, 2004, **108**, 19912.
34 T. D. Joseph, M. Tanaka, A. J. Wilkinson, S. G. Roberts, *J. Nucl. Mater.*, 2007, **367-370**, 637.